JOURNAL OF PROPULSION AND POWER
Vol. 19, No. 5, September–October 2003

Conceptual Study of a Combined-Cycle Engine for an Aerospace Plane

Takeshi Kanda* and Kenji Kudo†
National Aerospace Laboratory of Japan, Miyagi 981-1525, Japan

Operating conditions and performances of a fixed-geometry combined-cycle engine for a single-stage-to-orbit aerospace plane were calculated with a simple simulation model. With the flow conditions calculated with the model, the cooling requirement of the engine and pitching moment of the plane were investigated. The engine was composed of an ejector-jet mode, a ramjet mode, a scramjet mode, and a rocket mode. The engine had a fixed geometry in its operation. Subsonic combustion was conducted with no second throat in the combustor under the ejector-jet mode and the ramjet mode. Propellants were liquid hydrogen and liquid oxygen. The coolant flow rate became larger than the fuel flow rate. The excessive flow rate decreased the specific impulse above Mach 9 and restricted application of the airbreathing engine mode up to Mach 11. The pitching moment of the plane would be balanced even in the space in the configuration with the combined-cycle engine mounted on the windward surface.

Introduction

SCRAMJET engines for an aerospace plane are now under investigation in various countries. Although the scramjet engine will show high performance when used in application to a single-stage-to-orbit (SSTO) aerospace plane, other engines will be necessary for the SSTO plane to reach orbit. Therefore, the combined-cycle engine has been studied. Study of the combined-cycle engine has a long history, and several kinds of such engines have been proposed and studied.[1–3] A well-known combined cycle engine is the rocket-based combined cycle engine (RBCC).[4,5] The RBCC is composed of ejector-jet mode, ramjet mode, scramjet mode, and rocket mode.

When several engines are mounted on a vehicle, it is termed a combination propulsion system.[6] Each engine of the system is predicted to show a performance higher than that of the combined-cycle engine. However, the engines of the system will be heavier. During operation of one engine, additional engines may add drag, and they will add deadweight when turned off. Although the combined-cycle engine will show lower performance at each operating mode, it will be lighter and will not induce additional drag.

At the National Aerospace Laboratory of Japan, a combined-cycle engine is presently being studied. It is composed of ejector-jet mode, ramjet-mode, scramjet mode, and rocket mode. Herein, the concept of our propulsion system and the methods of estimating the propulsion system performances are first explained. Then, calculated flow conditions, engine performances, and results of a flight simulation of the SSTO plane are presented.

In the scramjet, the cooling requirement is larger than the fuel flow rate.[7] In the combined-cycle engine, ejector rockets are further integrated. The cooling requirement may be greater than that in the scramjet engine. The calculated flow conditions in the engine were applied to clarify the cooling requirement of the combined-cycle engine.

The combined-cycle engine will be mounted on the windward surface of the SSTO plane to intake air precompressed by the airframe. Figure 1 shows the plane. The thrust vector of the engine will not be at the center of gravity, and the engine thrust will produce a pitching moment. Balance of the pitching moment is a problem in a low flight-dynamic-pressure condition with little aerodynamic control. The plane should balance the moment only with the thrust of the engine. Balance of the pitching moment in a vacuum is also discussed, based on the calculated flow conditions of the engine.

Received 3 December 2002; revision received 10 May 2003; accepted for publication 11 May 2003.

*Group Leader, Ramjet Propulsion Research Center, 1 Koganesawa, Kimigaya, Kakuda; kanda@kakuda-splab.go.jp. Senior Member AIAA.

†Senior Researcher, Ramjet Propulsion Research Center, 1 Koganesawa, Kimigaya, Kakuda, kudo@kakuda-splab.go.jp.

Combined-Cycle Engine and Its Operating Conditions

Figure 2 shows a schematic diagram of the operating conditions of the combined cycle engine. It is composed of ejector-jet, ramjet, scramjet, and rocket modes. The propellants are liquid hydrogen and liquid oxygen. There is no second throat in the combustor. Subsonic combustion with no second throat configuration was attained in the experiments of the ramjet mode operation.[8–10] The subsonic combustion with no second throat was attained by acceleration under subsonic combustion and growth of the boundary layer. Without the second throat, the mechanical system of the engine can be simplified, and the engine will be lighter. The present model engine has a fixed geometry in its operation.

Under the ejector-jet mode, the pressure of the air is increased with the ejector rocket exhaust in the divergent section. Not only the rocket engine itself but also the divergent section with the increased pressure produce thrust. Subsonic combustion is attained by fuel injection from the second fuel injector. According to previous test results, mixing and combustion performances of the airbreathing rocket of subsonic combustion were significantly better than those of supersonic combustion.[8,11] In the ramjet mode, the rocket exhaust decreases, and pressure recovery of the air is attained in the divergent section. The recovered pressure is sufficient to produce thrust due to the high total pressure of the air. In the present study, ejector rockets with a high mixture ratio and a low chamber pressure worked as a torch for the downstream combustor. In the scramjet mode, the ejector rockets worked as a preburner to supply hot, fuel-rich gas.

Figure 3 is a three-dimensional image of the combined-cycle engine based on the present conceptual study. Ejector rockets are mounted on the top wall. The second fuel injectors used for subsonic combustion are located in the divergent section. A propellant feed system with umbilical ducts from the cryogenic propellant tanks will be mounted in the ejector rocket section. This is the heaviest section of the engine and will be difficult to move. In the model, this section and the following combustor section are fixed. The contraction of the inlet is also fixed. The inlet has a ramp-compression system. The ramp is movable and closes the inlet in the entry mode.

Simulation Methods

SSTO Plane Configuration and Boundary Layer

Figure 4 shows the configuration of the SSTO aerospace plane and the engine used in the present investigation. The length of the

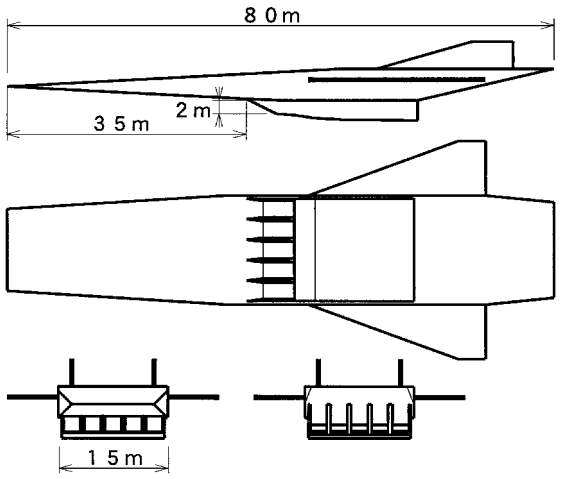

Fig. 1 Schematic image of SSTO aerospace plane.

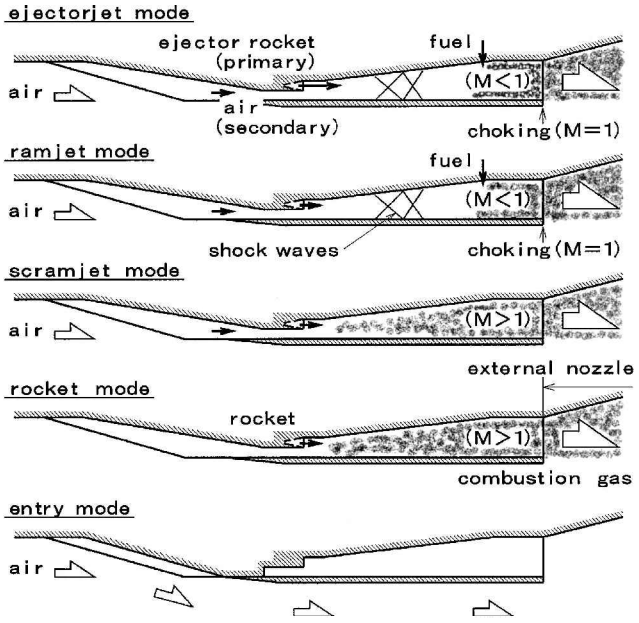

Fig. 2 Schematic diagram of operating conditions of the combined-cycle engine.

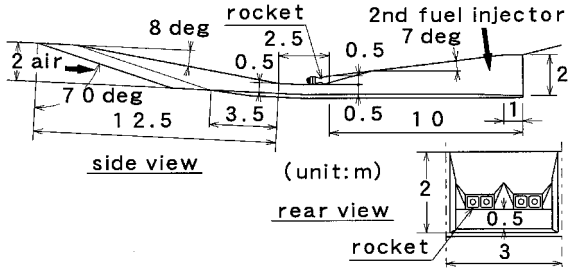

Fig. 3 Three-dimensional image of the combined-cycle engine, based on present study.

plane was 80 m. The length from the leading edge of the airframe to the engine was 35 m. The width of the plane body was 15 m, the engine length was 25 m, and the external nozzle was 20 m. Both the windward surface and the leeward surface of the airframe forebody were 3 deg from the airframe axis. There were five engine modules on the windward surface of the plane. The height of the engine was 2 m at both the entrance and the exit. In flight at Mach 12 with a deflection angle of 6 deg to the fight direction, a shock wave passed just below the inlet. The height of the airframe, that is, the height of the external nozzle, was 5 m. The width of the leading edge of the airframe was 8 m, as shown in Fig. 1, which was sufficient to attain precompression of air for the engine in the hypersonic flight condition.[12]

The leading edge should be sharp to decrease drag and to increase mass and momentum of the airflow to the engine. The sharp leading edge can be actively cooled in the hypersonic flight condition and the entry condition from a low-earth orbit.[13,14] The body of the plane was covered by a passive thermal protection system (TPS) of ceramic tile.

The turbulent boundary layer on the windward surface of the airframe was calculated with an assumption of the one-seventh power velocity profile and with the friction coefficient calculated with the formula of White (Ref. 15, pp. 642–644). The primary flow was assumed to be two dimensional on a flat plate. In the subsonic airflow, the incoming air conditions were used for the conditions on the windward surface, whereas in the supersonic flow, airflow conditions after the shock wave from the airframe leading edge were used. According to United Aerospace Plane (NASP) criteria for the boundary-layer transition, the boundary layer was turbulent at the entrance of the engine.[16] The airflow rate into the engine before spillage in the inlet was calculated with the displacement thickness.

Engine Configuration and Operating Conditions

An engine with a highly variable configuration can attain excellent performance. However, variable parts and possible positions will be restricted in the actual engine. The smaller the number of variable parts, the simpler and lighter the engine will be. In the present model engine, the inlet geometry was fixed during flight in air. The inlet was assumed to be movable at the ramp top wall. The closed configuration of the inlet is as shown in the entry mode in Fig. 2. The combustor geometry was fixed, and there was no second throat at the exit of the engine. The operating conditions of the ejector rockets, for example, the mixture ratio and the chamber pressure, were fixed at several levels because the turbopump for propellant supply will have a restricted number of operating conditions. The fuel flow rate from the second injector was changed to attain sufficient thrust in the ejector-jet mode and the ramjet mode. Figure 4 indicates the names and dimensions of the engine components and includes a diagram of the regenerative-cooling system.

One-dimensional cycle analysis methods were used to calculate the state properties of the airflow and combustion gas flow in the engine. The expansion of the combustion gas in the external nozzle was calculated with the two-dimensional Prandtl–Meyer function. The combustion gas was in a condition of equilibrium in the engine and in a frozen condition in the external nozzle. The interaction between the airflow and the ejector rocket exhaust in the mixer section was simulated with the simplified model mentioned subsequently. The friction coefficient of the turbulent boundary layer on the engine was calculated by the formula of White[15] (pp. 642–644).

The following engine geometry and the operating conditions were designed for flight with a dynamic pressure of 50 kPa. There are many design parameters in the combined-cycle engine, and so further optimization and improvement of configuration and operating conditions will be necessary. With an increase in possible engine configurations or operating conditions, engine performance increases.

Inlet

The inlet had a ramp-compression system. The ramp angle was 8.3 deg, and the captured mass flow rate was calculated with the ramp shock in the supersonic flow condition. The contraction ratio was 5.0, which was fixed throughout the engine operation except in the inlet-closed condition in the entry mode. The swept back angle of the sidewall leading edge was 70 deg. The total pressure was maintained in the subsonic condition in the inlet, whereas the kinetic energy efficiency was 0.98 in the supersonic flow condition. In the unstart condition, a normal shock was located ahead of the inlet, and subsonic air flowed into the engine.

In the rocket mode, the engine performance was calculated for two inlet conditions, that is, the inlet-open condition and the inlet-closed

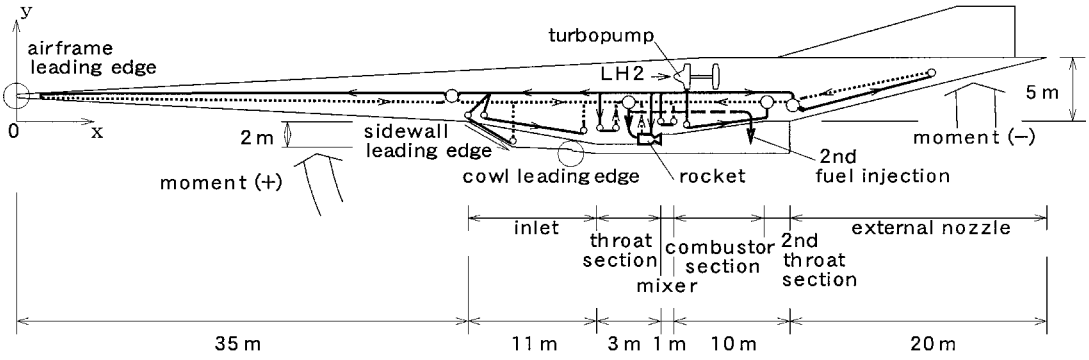

Fig. 4 Configuration of airframe and engine components. Schematic diagram of regenerative cooling system and direction of pitching moment are also shown.

condition. The inlet will be open for a long time in the rocket mode and will be closed during the ascent flight or in an orbit in a low flight-dynamic-pressure condition. However, the engine performance is better in the inlet-closed condition. Under the inlet-closed condition, the ramp top wall of the inlet moved and closed the inlet section, but the downstream components did not move in the present simulation model, as shown for the entry mode in Fig. 2.

Ejector Rocket

Each engine module had 4 ejector rockets, and thus, there were a total of 20 rockets on the vehicle. The throat diameter of the rocket was 0.14 m, and the nozzle area ratio of the ejector rocket was 9.5. The length of the combustion chamber was 0.3 m, and the characteristic length of the chamber, L^*, was 0.72. The mixture ratio of propellant oxygen and hydrogen, O/F, was 6.0 in the ejector–jet, ramjet, and rocket modes, whereas it was 0.5 in the scramjet mode. The specified mixture ratio was an averaged one. The pressure in the combustion chamber was 7.0 MPa in the ejector-jet and rocket modes. The pressure was 0.6 MPa in the ramjet and scramjet modes.

Mixer Section and Divergent Section

The contraction ratio of the mixer section based on the cross section at the engine entrance was 3.33, and the cross section at the end of the divergent section was the same as that at the engine entrance.

The interaction between the ejector jet and the suctioned air in the ejector-jet mode has been studied in detail in supersonic ejectors.[17–19] The interaction of momentum exchange in the mixer section was simulated with a simplified model. Figures 5a and 5b show schematic diagrams of the interaction between the rocket exhaust and the airflow. In the supersonic airflow condition, as shown in Fig. 5a, the high-pressure flow expands and the low-pressure flow contracts to the same static pressure. In the present model, the dividing streamline was represented by a straight line calculated at the initial condition of the interaction, using the two-dimensional Prandtl–Meyer function and the shock wave relation. The momentum was transferred through the line. After the interaction, the air and the rocket exhaust flowed in parallel one dimensionally at the same pressure with conservation of mass, impulse function, and energy.

In the subsonic airflow condition, as shown in Fig. 5b, the rocket exhaust flows through the expansion fan, and the dividing streamline inclines to the airflow. The dividing streamline curves gradually, and the line becomes parallel at the sonic point of the airflow. In the present model, first, pressure of the subsonic airflow at the entrance of the mixer section was assumed, and the airflow rate to the engine was calculated. The rocket exhaust expanded to the assumed pressure two dimensionally. The dividing streamline and the exchanged momentum were calculated, using the initial condition of the interaction under the pressure. The streamline was extended to the choking point of the airflow. After choking and the interaction, the air and the rocket exhaust flowed in parallel one dimensionally. The assumed pressure of the air was changed to conserve mass, impulse function, and energy. The exchanged momentum and the

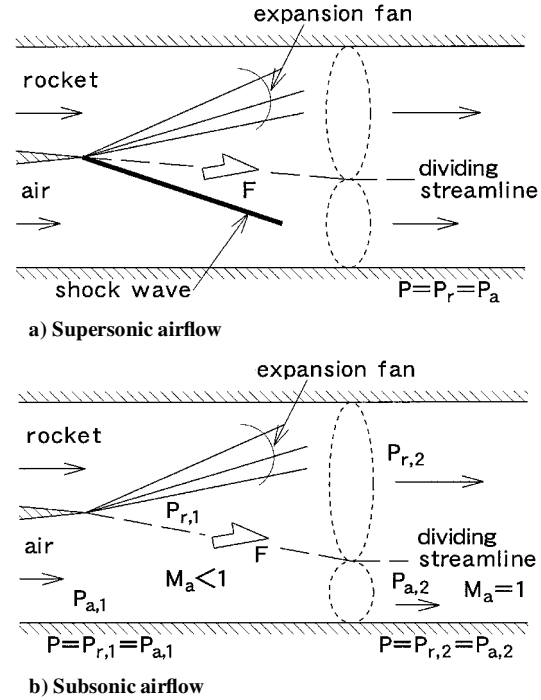

Fig. 5 Interaction between airflow and rocket exhaust in the mixer section of the ejector-jet mode.

airflow rate changed with the expansion angle of the rocket exhaust, which changed with the assumed airflow pressure. If the choking pressure of the subsonic airflow at the entrance of the mixer section was higher than the pressure of the rocket exhaust, the airflow was choked at the entrance of the mixer section, and the interaction was calculated in the same manner as that applied to the supersonic airflow.

The airflow and the rocket exhaust expanded isentropically and separately in the divergent section. The shock train was replaced with a normal shock wave. Downstream of the normal shock wave, the airflow and the rocket exhaust mixed. In the ramjet mode, the same procedure was adopted. In the scramjet mode, the rocket exhaust fully reacted with the air in the mixer section. The combustion gas expanded isentropically in the divergent section.

Under the inlet-open condition of the rocket mode, if there was airflow into the engine, the rocket exhaust further reacted with the air in the same manner as in the scramjet mode, and the combustion gas expanded in the divergent section. In the vacuum, combustion gas did not flow into the inlet, and the pressure in the inlet and the throat section was zero. The rocket exhaust expanded at the exit of the rocket nozzle with no reaction force to the mixer section duct, and then the gas expanded in the divergent section isentropically. Under the inlet-closed condition, the rocket exhaust expanded at the exit of the rocket nozzle into the mixer section duct, and the

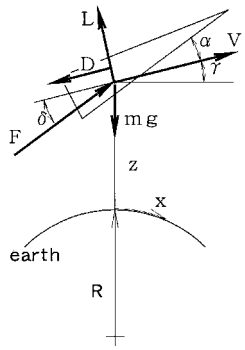

Fig. 6 Forces, velocity, and coordinates on aerospace plane.

pressure after the expansion acted in the throat section and at the end wall of the closed inlet. Then the gas expanded isentropically in the divergent section.

Second Fuel Injector and Choking Condition

In the ejector-jet and ramjet modes, subsonic combustion was attained with the fuel from the second injector, and the gas choked at the exit of the engine. The effective cross section, subtracting the displaced area by the boundary layer from the geometrical area, was used for choking. The displacement thickness of the turbulent boundary layer was calculated with an assumption of the one-seventh power velocity profile and the conservation of mass, impulse function, and energy. The combustor section was a straight duct and had the same cross section as that at the entrance of the engine.

Flight Simulation

The flight conditions with the combined cycle engine were investigated with a simulation of SSTO aerospace plane flight to a low-earth orbit of 100 km. The simulation methods of the flight of the plane were the same as those used in a previous investigation.[20] The initial mass of the aerospace plane was 460 Mg at takeoff. The aerospace plane was treated as a material point. The flight path was on a two-dimensional plane. The schematic diagram of the forces is shown in Fig. 6. In Fig. 6, x, R, z, v, γ, and α are distance on the Earth surface, the radius of the Earth, height, velocity, angle of inclination, and the angle of attack, respectively. F, δ, D, L, m, and g are force, angle between the engine thrust and the airframe velocity, drag, lift, mass, and acceleration of gravity at the height of z, respectively. The equations in the flight simulation are given as follows:

$$\frac{\mathrm{d}x}{\mathrm{d}t} = \frac{R}{R+z} \cdot v \cdot \cos\gamma \tag{1}$$

$$\frac{\mathrm{d}z}{\mathrm{d}t} = v \cdot \sin\gamma \tag{2}$$

$$\frac{\mathrm{d}v}{\mathrm{d}t} = \frac{F \cdot \cos\delta - D}{m} - g \cdot \sin\gamma \tag{3}$$

$$\frac{\mathrm{d}\gamma}{\mathrm{d}t} = \frac{F \cdot \sin\delta + L}{m \cdot v} - \frac{g \cdot \cos\gamma}{v} + \frac{v \cdot \cos\gamma}{R+z} \tag{4}$$

$$\frac{\mathrm{d}m}{\mathrm{d}t} = -\frac{F}{I_{\mathrm{sp}}} \tag{5}$$

In the equations, t, and I_{sp} are time and specific impulse defined in SI units. The aerodynamic data of the plane were from Ref. 21. The flight dynamic pressure was 50 kPa in the reference condition during the airbreathing propulsion mode.

Heat Flux from Air/Combustion Gas

The heat flux was calculated with Reynolds analogy. The heat flux at the leading edge with no swept back angle was calculated with the formula of Fay and Riddell.[22] Heat flux between the stagnation position and the downstream plate was calculated with the formula of Lees[23] (also see Ref. 15, pp. 596–605). Heat flux on the swept-back leading edge was calculated with the formula of Beckwith and Gallagher.[24] The radius of the leading edges was 0.005 m to reduce drag and to increase airflow to the engine. The wall temperature of the engine was set to be 1000 K except for the external nozzle and the airframe leading edge. Nickel alloy was assumed. If the total temperature was lower than the specified wall temperature, there was no heat flux to the wall. Although the wall temperature of the engine is higher than the inside insulator temperature,[25] the engine will be connected to the airframe by beams, and most heat will be conducted through them. Insulation of the inside environment of the vehicle from the engine will be possible. The heat flux of the ejector rockets was calculated with the formula of Bartz.[26] The heat flux in the rocket engine is high, especially around the throat, and the cooling jacket of many rockets is made of copper alloy with high thermal conductivity. The temperature of the rocket engine was set to be 800 K here.

Regenerative Cooling

The cooling requirement of the engine was calculated in a regenerative cooling system such as that shown in Fig. 4 with the estimated airflow and the combustion gas flow. Each engine module was cooled separately, and in a component, the top wall, sidewalls, and cowl were cooled separately. The combustor section was further divided into two sections in the direction of flow. The external nozzle was also divided into four sections in the direction of flow. Each cooling panel had coolant channels with a rectangular cross section. The cooling requirements of the leading edges of the sidewalls and the cowls were calculated separately from those of the plate components. The leading edge of the airframe was also cooled actively. The cooling channel of the leading edges was a circular pipe.

The engine was cooled with liquid hydrogen. The heat transfer to hydrogen was calculated with Taylor's correlation.[27] The friction factor of the coolant was calculated with a curve fit formula. (Ref. 15, pp. 486–487). The fin effect was included in the heat transfer calculation of the cooling jacket.[28] The wall thickness was 1 mm. The coolant hydrogen returned to the injector manifold of the ejector rockets or the second fuel injector at the divergent section. The properties of the liquid hydrogen were calculated with a computer code.[29]

Use of liquid hydrogen in the airframe cooling, for example, at the leading edge of the airframe and in the external nozzle, should be avoided for safety reasons. Moreover, because these components are far from the engine, there will be heat leakage during the movement of cryogenic liquid hydrogen if it is used for cooling. Study of cooling of the external nozzle with several coolants other than liquid hydrogen have already been conducted.[30] In the present study, the external nozzle and the leading edge of the airframe were cooled by Barrel Silicone Fluid® ST, a commercial product of Matsumura Oil Co., Ltd. Its range of use is 230–670 K. It is nontoxic, and its composition is stable. At the leading edge, the wall temperature at the stagnation position was set to be 600 K. The wall temperature of the external nozzle was set to be 500 K not to exceed the inside insulation foam temperature.[25] The absorbed heat was exchanged with liquid hydrogen.

The exit conditions of the cooling jacket of the ejector rockets were specified based on the operating conditions of the Japanese liquid hydrogen/liquid oxygen rocket engines, that is, the LE-5 and LE-7. The temperature of hydrogen at the exit of the jacket was 400 K, and the pressure drop in the jacket was 0.15 times the rocket chamber pressure. The drop in fuel injector pressure of the ejector rockets was 0.2 times the chamber pressure.

Pitching Moment

The pitching moment was investigated under the vacuum condition. The direction of the pitching moment is as shown in Fig. 4. The thrust of the ejector rocket acts in the headup direction. The thrust is large, but the moment arm is short. The thrust by the external nozzle acts in the headdown direction. The thrust is not large, but the moment arm is long. As the height of the external nozzle, that is, the height of the airframe, increases under the fixed length in

the x direction, the angle of the external nozzle increases, and the pressure on the nozzle decreases. Then the moment by the external nozzle decreases, and the pitching moment also decreases, although the projected area of the external nozzle increases. The origin of x was at the leading edge of the airframe, and that of y was at the bottom of the airframe.

The pitching moments of the two inlet conditions, that is, the inlet-open condition and the inlet-closed condition, were investigated. The contraction ratio of the inlet was 5.0 in the inlet-open condition. The contraction ratio of the throat section was also 5.0 in the inlet-closed condition; the inlet section, however, was closed. The rocket engine force point was $x = 48$ m from the leading edge of the airframe and $y = -1.5$ m from the bottom of the airframe.

Results and Discussion

Engine Thrust Performances and Operating Conditions

Figures 7a–7c show the specific impulse, the thrust coefficient, and the mixture ratio of propellant oxygen and hydrogen, respectively. Figures 8a–8f show the flow conditions in the engine. The angle of attack was 3 deg. The thrust coefficient was large around the Mach 0 condition because the thrust was nondimensionalized by dynamic pressure. In the scramjet mode, as mentioned in the next paragraph, hydrogen flow rate for cooling became larger than the rate for fuel. The specific impulse was calculated with and without the cooling fuel flow rate, and the thrust was calculated without the cooling fuel flow. The impulse with the cooling fuel flow is indicated with "cooling fuel flow" in Fig. 7a. The mixture ratio with the coolant fuel flow in the scramjet mode is also plotted in Fig. 7c. The results and their tendencies resembled those of the others.

Around Mach 4, there were three operating conditions, that is, the ejector-jet mode with the inlet-unstarted condition (Fig. 8b), the ejector-jet mode with the inlet-started condition (Fig. 8c), and the ramjet mode (Fig. 8d). The inlet has hysteresis between the started and the unstarted conditions.[31] The unstarted condition would continue to higher Mach number with increasing flight Mach number during ascent flight.

Under the ejector-jet mode with the inlet-started condition, the thrust was large, and the specific impulse was moderate. In this condition, the terminal shock wave was located just downstream of the entrance of the divergent section. The drag in the inlet was small, and the pressure in the combustor was high. Under the ejector-jet mode with the inlet-unstarted condition, the shock wave was just upstream of the exit of the divergent section. The pressure in the inlet was high, and the drag in the inlet was large. The pressure in the combustor was low. Therefore, the thrust and the specific impulse were low.

The operating conditions of the engine and the configurations, especially in the ejector-jet mode and the ramjet mode, depended on the flight corridor, for example, the design flight-dynamic pressure. If the flight-dynamic pressure changes, the engine geometry and the rocket engine operating conditions should be changed.

Cooling Requirement

Figure 9 shows distributions of the radius of the ejector rocket and the heat flux at a chamber pressure of 7 MPa and a mixture ratio of O/F = 6. The heat flux was highest at the throat up to about 50 $MW \cdot m^{-2}$. Figure 10 shows the cooling requirements in the ejector-jet mode at a flight Mach number of 0.5; in the ramjet mode at Mach 5; in the scramjet mode at Mach 8, 10, and 12; and in the rocket mode in vacuum under the inlet-open condition. The coolant was nondimensionalized with the fuel hydrogen flow rate. The cooling requirement of the airframe leading edge was included in the airbreathing engine part. In the ejector-jet mode, the calculated pressure on the external nozzle was lower than the ambient pressure. Therefore, the combustion gas was assumed to separate in the external nozzle, and the cooling requirement of the external nozzle became zero.

In the ramjet and scramjet modes, the cooling requirement at the external nozzle was high due to the low wall temperature of 500 K. In the rocket mode, although there was no secondary fuel injection and the fuel flow rate was different from that in the ejector-jet mode, the operating conditions of the ejector rocket were the same as those in the ejector-jet mode. The combustion gas did not separate from the external nozzle. In the scramjet mode, the cooling requirement was high in the airbreathing engine part due to the high total temperature of the air.

In the scramjet mode, the cooling requirement exceeded the fuel hydrogen flow rate above Mach 9, although the cooling requirement of the ejector rocket was small in the scramjet mode due to low pressure and temperature in the rocket chamber. The cooling fuel flow rate became 1.6 times as large as the fuel flow rate at Mach 12.

The required hydrogen supply pressure was 9.5 MPa in the ejector-jet and rocket modes, due to the high pressure of the rocket chamber of 7 MPa. In the ramjet mode, the supply pressure was 3.5 MPa. In the scramjet mode, the pressures were 4.7 MPa at Mach

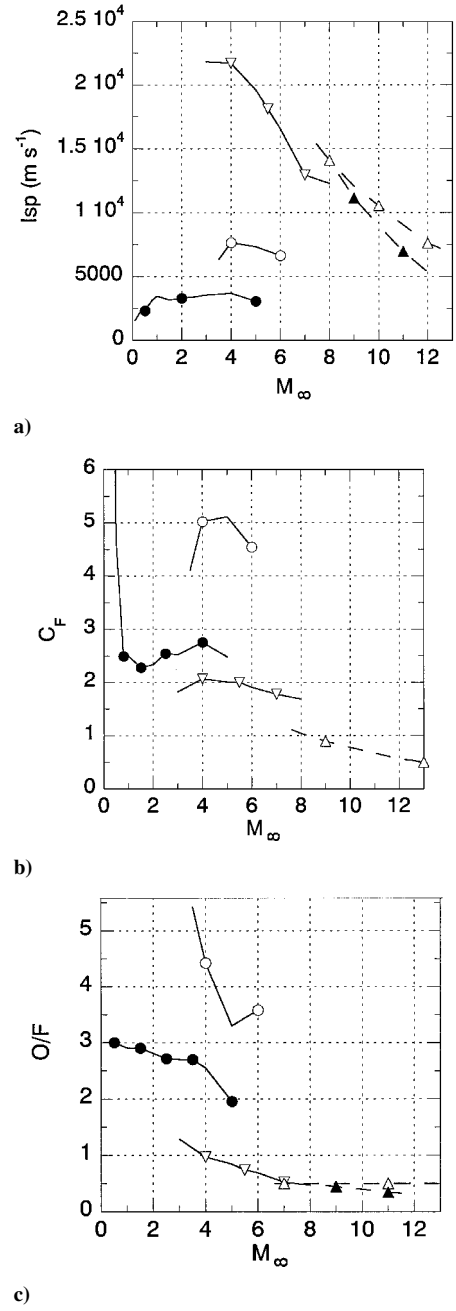

Fig. 7 Engine performances of the combined cycle engine: a) Specific impulse, where 'cooling fuel flow' of the scramjet mode is impulse based on the cooling fuel flow rate for the regenerative cooling: ●, ejector jet (supersonic unstart); ○, ejector jet (supersonic start); ▽, ramjet; △, scramjet; and ▲, scramjet (cooling fuel flow); b) thrust coefficient, and c) mixture ratio O/F.

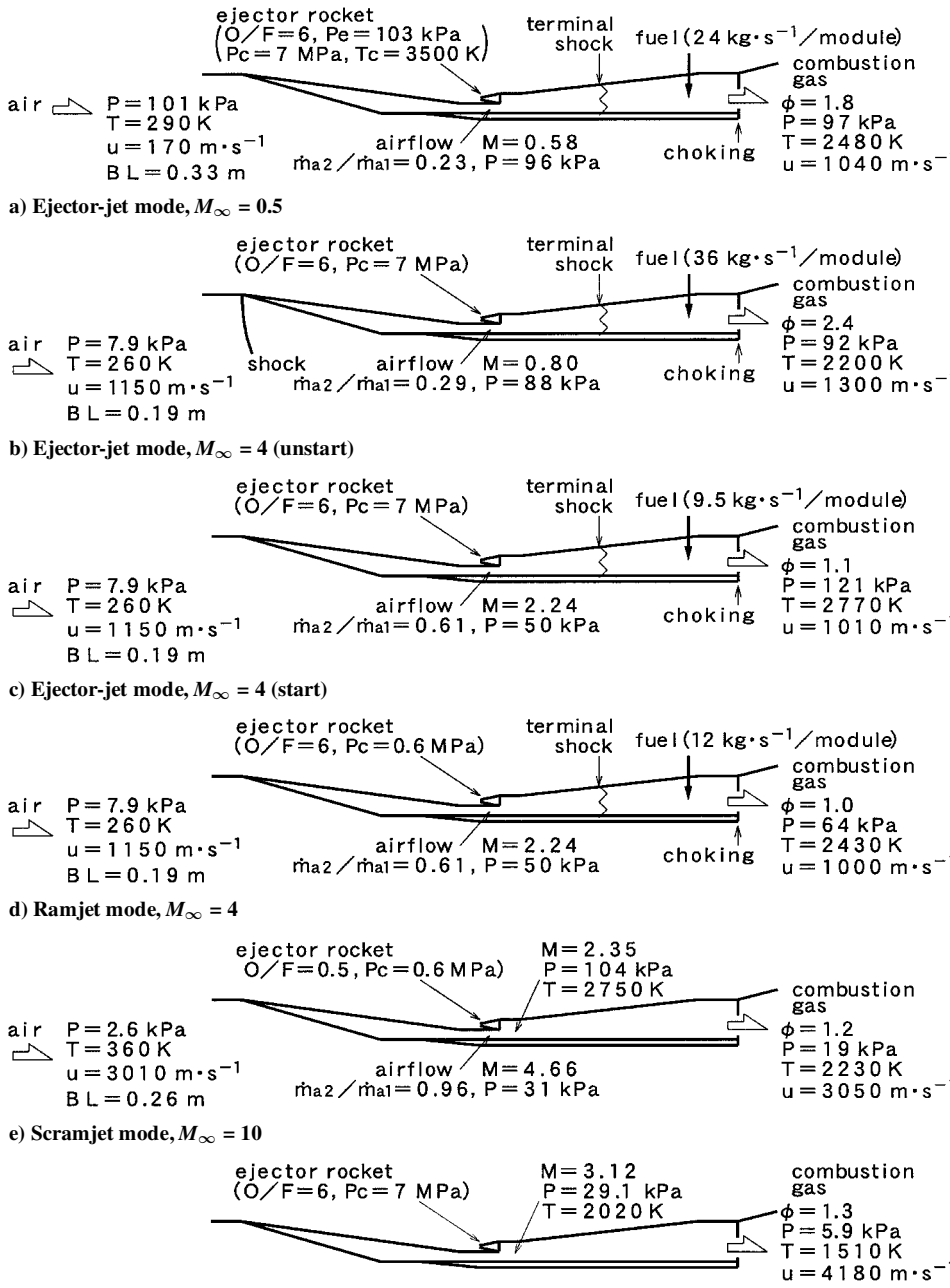

Fig. 8 Operating conditions of the combined cycle engine.

10 and 6.9 MPa at Mach 12. Although the rocket chamber pressure was low, the pressure in the hydrogen injector manifold had to be 3 MPa in the ramjet and scramjet modes to avoid abrupt changes in property around the critical point of hydrogen. The pump supply pressure of the cooling system was not so high. The moderate pressure level was within the reasonable range of reusable engines.

Fight Simulation

Figure 11 shows the flight condition of the SSTO plane with the combined-cycle engine to a low-earth orbit of 100 km. The trajectory was along the flight-dynamic pressure of 50 kPa, except at takeoff. In this simulation, the ejector-jet mode was up to Mach 3. In the ejector-jet mode, the inlet was unstarted in the supersonic condition. The ramjet mode was from Mach 3 to Mach 7. The scramjet mode was from Mach 7 to Mach 11, using the specific impulse with the cooling fuel flow. In the rocket mode, the inlet was open.

The average specific impulse of the combined-cycle engine, which was calculated with the impulse from takeoff to the orbit and the consumed propellant amount, was 5160 $m \cdot s^{-1}$. The flight time was shorter than that of the combination engine system with the air-turbo-ramjet, the scramjet, and the rocket.[20] The shorter flight time was caused by larger thrust of the combined cycle engine. The shorter the flight time, the lighter the TPS weight of the plane surface will be. The mass carried into the orbit was 67 Mg. When the specific impulse without cooling fuel flow was used, the mass into the orbit became 68 Mg with the scramjet mode up to Mach 12. The engine weight was estimated to be 14 Mg under the assumption that the weight was a sum of the scramjet and the rocket.[20,32] The mass carried into orbit will increase with optimization of the configuration and the operating conditions of the engine.

Pitching Moment (1)

Balance of the pitching moment in the vacuum condition in the rocket mode was investigated with several parameters. In the reference condition, the x coordinate of the gravity center, $x_{g.c.}$, was 40 m from the leading edge in the horizontal direction, which was

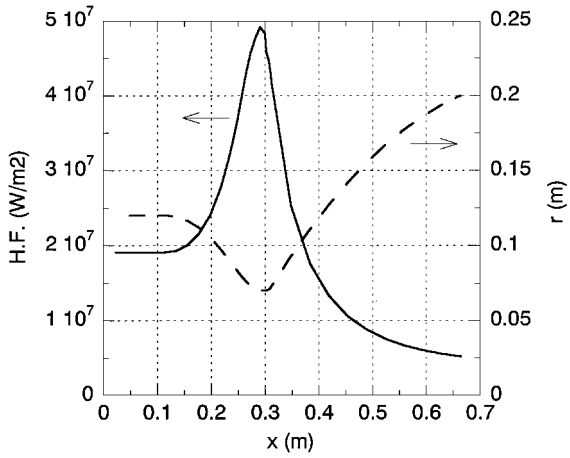

Fig. 9 Heat flux and radius of ejector rocket at a chamber pressure of 7 MPa and O/F = 6.

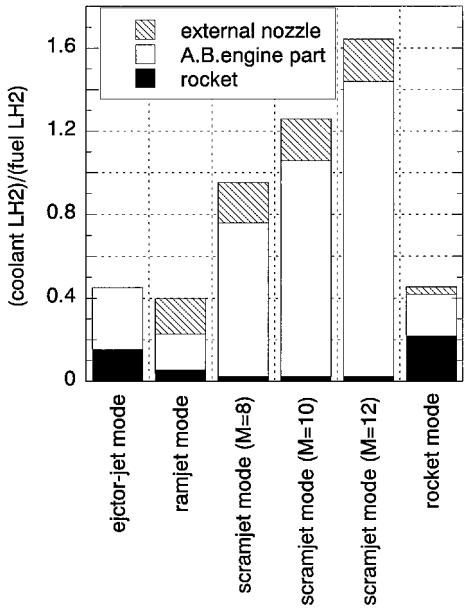

Fig. 10 Cooling requirements of the combined-cycle engine.

half the length of the airframe, $x_{g.c.}/L_{AF} = 0.5$. The y coordinate of the gravity center, $y_{g.c.}$, was 0 m from the bottom of the airframe, which was the top of the engine. The mixture ratio of the rocket was O/F = 6.0. The moment was nondimensionalized by the product of the rocket engine thrust and half of the airframe height.

The effect of the position of the gravity center is shown in Figs. 12a and 12b. In Fig. 12a, $y_{g.c.}/H_{AF} = 0$. As the gravity center changed downstream, the distance between the external nozzle and the gravity center became short, and the moment by the external nozzle decreased. The moment was balanced around $x_{gc}/L_{AF} = 0.6$. In the inlet-closed condition, pressure acted on the end wall of the closed inlet section, and the positive moment was larger than that under the inlet-open condition. In Fig. 12b, $x_{g.c.}/L_{AF} = 0.5$. The moment was balanced around $y_{g.c.}/H_{AF} = 0.2$, just above the airframe bottom.

Figure 13 shows the effect of the height of the external nozzle, H_{EN}. The height of the external nozzle was equal to that of the airframe here. The gravity center was located at the reference position. As the height of the external nozzle increased, the nozzle angle increased, and the pressure on the nozzle surface decreased. Then the negative moment by the external nozzle became small, and the net moment increased.

As shown in Figs. 12 and 13, the pitching moment was around zero in the present configuration of the plane and the engine. Therefore, the pitching moment will be canceled out even in the vacuum

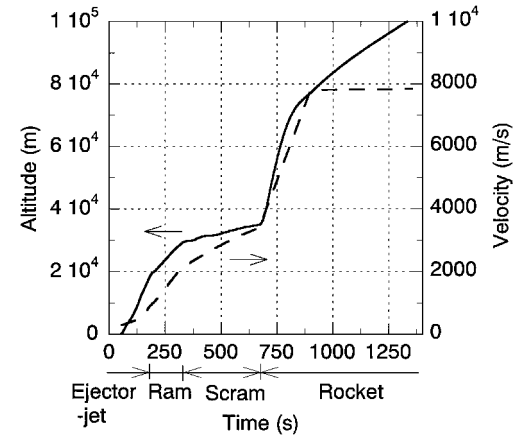

Fig. 11 Flight condition of SSTO plane with the combined-cycle engine. Specific impulse with cooling fuel flow rate was used in scramjet mode.

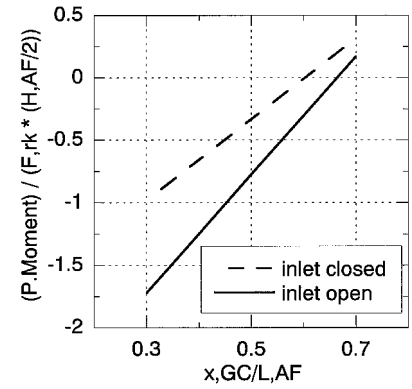

a) *x* direction

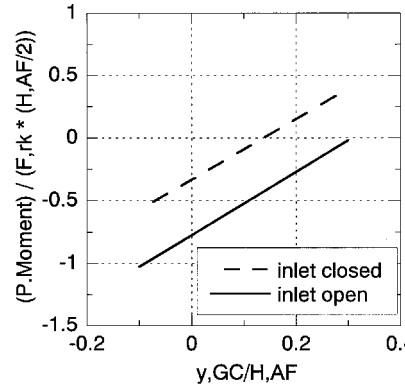

b) *y* direction

Fig. 12 Effects of the position of the gravity center on pitching moment of the SSTO plane.

condition in such an SSTO plane in which the engine is mounted on the windward surface.

Pitching Moment (2)

In actual flight, the flight condition will change during the transition of the engine operating modes. Here, to grasp an overview of the pitching moment change at the mode transition, change of the pitching moment from the scramjet mode to the rocket mode was calculated at a fixed Mach number of 11 and a fixed flight dynamic pressure of 50 kPa. The effect of the aerodynamic components, for example, the wings, was not included, but the effect of the airframe was. The inlet was open with a contraction ratio of five. The airflow condition around the airframe was calculated with the two-dimensional shock wave relations and the two-dimensional Prandtl–Meyer function. The ejector rocket operating condition moved from

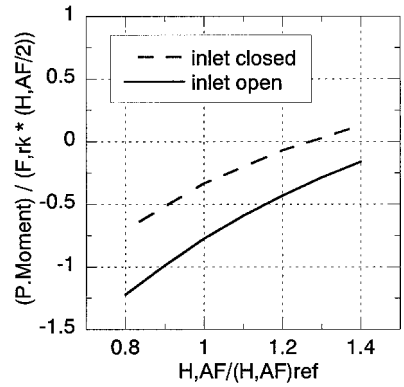

Fig. 13 Effect of height of external nozzle on pitching moment of the SSTO plane.

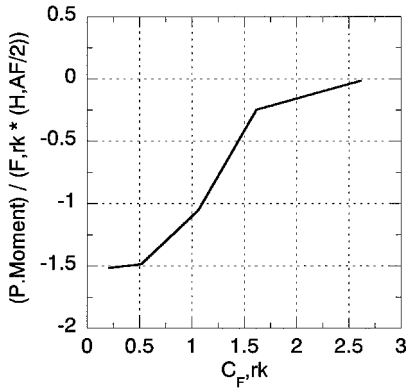

Fig. 14 Pitching moment change from scramjet mode to rocket mode at Mach 11.

[*Pc* (MPa), O/F] = (0.6, 0.5) of the scramjet mode to (6, 7) of the rocket mode. The transient conditions were (1.5,1.5), (3.0,3.0), and (4.5, 4.5).

The calculated result is shown in Fig. 14. The thrust coefficient of the rocket, $C_{F,\mathrm{rk}}$, was calculated with the flight-dynamic pressure of 50 kPa and the engine cross section at the entrance. The pitching moment was nondimensionalized with one-half of the airframe height and the reference rocket thrust. In Fig. 14, the point on the left-hand side indicates the scramjet mode, and that on the right-hand side indicates the rocket mode.

The contributions of the aerodynamic forces, especially, the positive moment from the windward forebody surface, were large. However, in the scramjet mode, the moment from the external nozzle was large, and the pitching moment was negative. Wings to balance the moment are necessary. As the rocket thrust increased, the contribution of the rocket engine became large, and the pitching moment approached to zero. The SSTO plane still flies higher during the transition from the scramjet mode to the rocket mode, and the moment by aerodynamic forces decreases in flight of the rocket mode. As shown in Figs. 12 and 13, the plane will be designed to balance the pitching moment in a vacuum. The positive moment of the rocket mode will become zero during ascent flight to orbit.

Conclusions

Engine performances of a fixed-geometry combined-cycle engine for an aerospace plane were calculated using a simplified model simulation. The engine was composed of ejector-jet, ramjet, scramjet and rocket modes. In the ejector-jet mode, subsonic combustion was adopted. Propellants were liquid hydrogen and liquid oxygen. Liquid hydrogen was used for active cooling.

The required coolant flow rate, which was largest in the scramjet mode, was larger than the fuel hydrogen flow rate in the Mach number larger than 9. The application of the regenerative cooling to the combined-cycle engine reduced the specific impulse and the effective operating range of the airbreathing engine mode. The pressure of supplied hydrogen, which was highest in the ejector-jet and rocket modes, was not so high. The pressure level was within the reasonable range for reusable engines.

The pitching moment would be balanced even in the vacuum condition in the plane configuration with the engine mounted on the windward surface.

Acknowledgments

The authors appreciate the diligent work of Yoshinari Enomoto of Kawasaki Heavy Industries, Ltd., in the survey of coolants. The authors thank Keisuke Fujii of the National Aerospace Laboratory of Japan for the discussion on the boundary layer. The authors used a code for cooling requirements of the rocket engine by Yoshio Wakamatsu of the National Aerospace Laboratory of Japan.

References

[1]Escher, W. J. D., "A User's Primer for Comparative Assessments of All-Rocket and Rocket-Based Combined-Cycle Propulsion Systems for Advanced Earth-to-Orbit Space Transport Applications," AIAA Paper 95-2474, July 1995.

[2]Olds, J. R., and Bradford, J. E., "SCCREAM: A Conceptual Rocket-Based Combined-Cycle Engine Performance Analysis Tool," *Journal of Propulsion and Power*, Vol. 17, No. 2, 2001, pp. 333–339.

[3]Heiser, W. H., Pratt, D. T., Daley, D. H., and Mehta, U. B., *Hypersonic Airbreathing Propulsion*, AIAA Education Series, AIAA, Washington, DC, 1994, pp. 447–451.

[4]Faulkner, R. F., "Integrated System Test of an Airbreathing Rocket (ISTAR)," AIAA Paper 2001-1812, April 2001.

[5]Siebenhaar, A., "Strutjet Evolves to Meet Air-Breathing Propulsion Challenges for the 21st Century," *Proceedings of the 13th International Symposium on Airbreathing Engines*, ISABE Paper 97-7135, Sept. 1997.

[6]Bertin, J. J., *Hypersonic Aerothermodynamics*, AIAA Education Series, AIAA, Washington, DC, 1994, pp. 592-594.

[7]Kanda, T., Masuya, G., and Wakamatsu, Y., "Propellant Feed System in a Regeneratively Cooled Scramjet," *Journal of Propulsion and Power*, Vol. 7, No. 2, 1991, pp. 299–301.

[8]Masuya, G., Chinzei, N., and Ishii, S., "A Study of Air Breathing Rockets—Subsonic Mode Combustion," *Acta Astronautica*, Vol. 8, No. 5-6, 1981, pp. 643–661.

[9]Kanda, T., Chinzei, N., Kudo, K., and Murakami, A., "Dual-Mode Operation in a Scramjet Combustor," AIAA Paper 2001-1816, April 2001.

[10]Kato, K., Kanda, T., Kudo, K., and Murakami, A., "Ramjet-mode Operation in a Scramjet Combustor," *Proceedings of the 16th International Symposium on Airbreathing Engines*, ISABE Paper 2003-1150, Sept. 2003.

[11]Chinzei, N., Masuya, G., Kudo, K., Murakami, A., and Komuro, T., "An Experimental Study of Multiple Fuel Supplies into the Secondary Combustor of Air Breathing Rockets," *Proceedings of 7th International Symposium on Airbreathing Engines*, AIAA, Reston, VA, 1985, pp. 561–568.

[12]Kodera, M., Kanda, T., and Tani, K., "Effect of Airframe Geometry on Thrust Performance of Aerospace Plane," AIAA Paper 2000-3342, July 2000.

[13]Kanda, T., and Kudo, K., "Preliminary Study of Thermal Protection System of a Single-Stage-to-Orbit Plane," *Proceedings of the 22nd International Symposium on Space Technology and Science*, Japan Society for Aeronautical and Space Sciences, Tokyo, 2000, pp. 1354–1360.

[14]Kudo, K., and Kanda, T., "Preliminary Study of Thermal Protection System of a Single-Stgae-to-Orbit Plane (II)," *Proceedings of the 23rd International Symposium on Space Technology and Science*, Japan Society for Aeronautical and Space Sciences, Tokyo, 2002, pp. 1075–1080.

[15]White, F. M., *Viscous Fluid Flow*, McGraw–Hill, New York, 1974, pp. 486–487, 596–605, 642–644.

[16]Berry, S. A., Auslender, A. H., Dilley, A. D., and Calleja, J. F., "Hypersonic Boundary Layer Trip Development for Hyper-X," *Journal of Spacecraft and Rockets*, Vol. 38, No. 6, 2001, pp. 853–864.

[17]Chow, W. L., and Addy, A. L., "Interaction Between Primary and Secondary Streams of Supersonic Ejector Systems and Their Performance Characteristics," *AIAA Journal*, Vol. 2, No. 4, 1964, pp. 686–695.

[18]Fabri, J., and Siestrunck, R., "Supersonic Air Ejectors," *Advances in Applied Mechanics*, Vol. 5, Academic Press, New York, 1958, pp. 1–34.

[19]Aoki, S., Lee, J., Masuya, G., Kanda, T., Kudo, K., and Murakami, A., "Experimental Investigation of Ejector-Jet," AIAA Paper 2003-0188, Jan. 2003.

[20]Kanda, T., and Kudo, K., "Payload to Low Earth Orbit by Aerospace Plane with Scramjet Engine," *Journal of Propulsion and Power*, Vol. 13, No. 1, 1997, pp. 164–166.

[21]Nomura, S., Hozumi, K., and Kawamoto, I., "Experimental Studies on Aerodynamic Characteristics of SSTO Vehicle at Subsonic to Hypersonic Speeds," *Proceedings of the 16th International Symposium on Space Technology and Science*, Japan Society for Aeronautical and Space Sciences, Tokyo, 1988, pp. 1547–1554.

[22]Fay, J. A., and Riddell, F. R., "Theory of Stagnation Point Heat Transfer in Dissociated Air," *Journal of Aeronautical Sciences*, Vol. 25, No. 2, 1958, pp. 73–85, 121.

[23]Lees, L., "Laminar Heat Transfer Over Blunt-Nosed Bodies at Hypersonic Flight Speeds," *Jet Propulsion*, Vol. 26, No. 4, 1956, pp. 259–269.

[24]Beckwith, I. E., and Gallagher, J. J., "Local Heat Transfer and Recovery Temperature on a Yawed Cylinder at a Mach Number of 4.15 and High Reynolds Numbers," NASA TR R-104, 1958.

[25]Lockwood, M. K., Hunt, J. L., and Martin, J. G., "Airbreathing Hypersonic Vehicle Design and Analysis Methods," AIAA Paper 96-0381, Jan. 1996.

[26]Bartz, D. R., "A Simple Equation for Rapid Estimation of Rocket Nozzle Convective Heat Transfer Coefficients," *Jet Propulsion*, Vol. 27, No. 1, 1957, pp. 49–51.

[27]Taylor, M. F., "Correlation of Local Heat-Transfer Coefficients for Single-Phase Turbulent Flow of Hydrogen in Tubes with Temperature Ratios to 23," NASA TN D-4332, Jan. 1968.

[28]Eckert, E. R. G., and Drake, R. M., Jr., *Analysis of Heat and Mass Transfer, McGraw–Hill*, New York, 1972, pp. 78–85.

[29]Hendricks, R. C., Baron, A. K., and Peller, I. C., "GASP—A Computer Code for Calculating the Thermodynamic and Transport Properties for Ten Fluids: Parahydrogen, Helium, Neon, Methane, Nitrogen, Carbon Monoxide, Oxygen, Fluorine, Argon, and Carbon Dioxide," NASA TN D-7808, Feb. 1975.

[30]Jones, S., and Petley, D., "A Comparison of Cooling Methods for the Airframe Nozzle of a Single-Stage-to-Orbit Aircraft," AIAA Paper 91-5036, Dec. 1991.

[31]Van Wie, D. M., Kwok, F. T., and Walsh, R. F., "Starting Characteristics of Supersonic Inlets," AIAA Paper 96-2914, July 1996.

[32]Glatt, C. R., "WAATS—A Computer Program for Weight Analysis of Advanced Transportation Systems," NASA CR-2420, Sept. 1974.